ADVANCED ENERGY & SUSTAINABILITY RESEARCH
Open Access
www.advenergysustres.com

Improvement of Catalytic Methane Oxidation by Nitric Acid Treatment on Pt/TiO_2

*Jiseok Park, Wo Bin Bae, Sang Woo Byun, Hyeonwoo Shin, Haehyun Min, Young Jin Kim, and Sung Bong Kang**

This study investigates the effect of nitric acid (Pt:NA) treatment on the catalytic performance of Pt/TiO_2 catalysts in methane oxidation. By varying the molar ratio of Pt to nitric acid (NA) from 1:0.1 to 1:10 of Pt:NA, a series of Pt/NA-TiO_2 catalysts are synthesized. The structural and catalytic properties are identified using X-Ray photoelectron spectroscopy, transmission electron microscopy, and diffuse reflectance infrared Fourier transform spectroscopy. The NA treatment during the catalyst synthesis promotes the formation of acidic sites, enhancing the uniform adsorption of the Pt precursor, which in turn improves Pt dispersion and catalytic activity. However, excessive NA treatment above Pt:NA ratio of 1:5 induces the formation of larger Pt particles due to competitive nitrate adsorption, leading to decreased Pt dispersion and diminished catalytic performance. These findings provide a simple method for synthesizing active Pt supported on TiO_2 catalysts with NA treatment having well-dispersed Pt particles, thereby maximizing the catalytic activity of the methane oxidation.

1. Introduction

Methane (CH_4), a potent greenhouse gas, exhibits a global warming potential ≈20 times greater than carbon dioxide (CO_2).[1] Developing highly efficient catalysts to oxidize methane into CO_2 is crucial for addressing environmental concerns and mitigating climate change. However, the oxidation of methane presents significant challenges, particularly due to the strong C—H bond in CH_4, which has a bond dissociation energy of 104 kcal mol^{-1}, and the presence of high concentrations of water vapor (5–15%) in various environmental contexts.[2,3] A deeper understanding of catalyst design and behavior under these conditions is imperative for advancing methane oxidation technologies, as it could also inform the development of catalysts for other oxidation reactions across diverse applications.

The support material in catalytic systems plays a critical role in influencing both the behavior of the active metal and the overall reaction mechanism.[4–6] Therefore, it is vital to develop methodologies to assess the influence of support materials on catalytic performance comprehensively. Catalysts are essential in addressing global environmental issues, such as reducing emissions and improving energy conversion efficiency. Understanding the interactions between active sites and support materials provides an avenue for optimizing catalytic activity and stability, which is crucial for the effectiveness of catalysts in real-world applications.

Platinum group metals, particularly platinum (Pt), are highly regarded as promising candidates for oxidation catalysis due to their superior catalytic properties.[7,8] While methane oxidation studies have traditionally focused on palladium (Pd), which exhibits high activity, its performance is significantly hindered in the presence of water vapor, limiting its practical applications.[9] Consequently, research has shifted toward platinum, which shows reduced sensitivity to water inhibition and offers enhanced performance in methane oxidation, making it a more viable option in various conditions.[10] Pt-based catalysts have shown that the catalytic performance is highly dependent to the characteristics of support. For instance, Pt/SiO_2-Al_2O_3 catalysts have demonstrated higher activity in methane oxidation compared to Pt/Al_2O_3, primarily due to improved oxygen mobility and better interaction with the reactants.[11] Furthermore, Pt supported on CeO_2-ZrO_2 solid solutions exhibits superior

---

J. Park, S. W. Byun, H. Shin, S. B. Kang
Research Center for Innovative Energy and Carbon Optimized Synthesis for Chemicals (Inn-ECOSysChem), School of Environment and Energy Engineering
Gwangju Institute of Science and Technology
Gwangju 61005, Republic of Korea
E-mail: sbkang@gist.ac.kr

W. B. Bae
Department of Chemical Engineering
Rowan University
Glassboro, NJ 08028, USA

H. Min
Department of Chemical Engineering
State University of New York College of Environmental Science and Forestry
Syracuse, NY 13210, USA

Y. J. Kim
Department of Environmental Engineering
Kyungpook National University
80 Daehak-ro, Daegu 41566, Republic of Korea

The ORCID identification number(s) for the author(s) of this article can be found under https://doi.org/10.1002/aesr.202400358.

DOI: 10.1002/aesr.202400358

performance at lower temperatures compared to Pt/Al_2O_3; however, deactivation occurs above 250 °C, indicating the importance of thermal stability in catalyst design.[12]

Acidic supports, such as TiO_2, significantly enhance catalytic activity, as evidenced by the lower T_{50} (the temperature at which 50% of the reactant is converted) observed in Pt/TiO_2 catalysts compared to Pt/SiO_2.[13,14] Moreover, TiO_2-based catalysts offer significant promise due to their versatile properties and ability to support active metal sites, such as Pt, across a variety of oxidation reactions. Their high surface area, stability, and tunable surface chemistry make TiO_2 an ideal support for enhancing both the activity and durability of oxidation catalysts. This highlights opportunities for further optimization and industrial application, particularly in catalytic methane oxidation, which is crucial for reducing greenhouse gas emissions. Under acidic conditions below the point of zero charge (PZC), the TiO_2 surface becomes protonated, resulting in positively charged hydroxyl groups ($-OH_2^+$), which generate surface charge and provide anchoring points for Pt precursor adsorption.[15] These acidic sites enhance Pt dispersion across the support by promoting uniform Pt precursor distribution, thus preventing Pt particle aggregation during calcination.[16] Conversely, insufficient acidic sites lead to localized clustering of Pt precursors, resulting in larger Pt particles and reduced catalytic performance.

Given the versatility of TiO_2 as a catalyst support, this study unveiled the impact of nitric acid (NA) treatment on the structural and catalytic properties of Pt/TiO_2 in methane oxidation. Specifically, we investigated the role of surface acidity, Pt particle size, dispersion, and oxidation states to optimize the catalytic performance of Pt/TiO_2. By systematically analyzing the surface functional groups, redox properties, and acid site distribution, this study provides insights into a simple methodology with the NA treatment of TiO_2 for improving methane oxidation.

2. Results and Discussions

2.1. Effect of NA Treatment on Acidic Site Formation

The Pd content of the catalysts was determined using Inductively coupled plasma optical emission spectroscopy to verify the actual loading. As summarized in Table S1 in the Supporting Information, the Pd content across all samples ranged from 1.8 to 2.1 wt%, demonstrating consistent incorporation regardless of the NA treatment concentration. The Braunauer–Emmett–Teller (BET) surface area (S_{BET}) and total pore volume were measured via N_2 adsorption–desorption isotherms. The S_{BET} values varied between 56.4 and 62.6 $m^2\,g^{-1}$, while the total pore volume ranged from 0.25 to 0.28 $cm^3\,g^{-1}$, suggesting that NA treatment did not significantly alter the surface area or porosity of the TiO_2 support. These results indicate that NA treatment has minimal impact on the overall Pd content and textural properties of the support.

The ammonia temperature-programmed desorption (NH_3-TPD) profiles provide a detailed insights into the formation of acidic sites following NA treatment on TiO_2 as compared in Figure S1 in the Supporting Information. The DI-TiO_2, treated with deionized (DI) water, was employed as the baseline support, displaying weak acid sites around 200 °C. This indicates minimal surface acidity in the untreated state of TiO_2. However, after NA treatment, NA-TiO_2 (1:1) and NA-TiO_2 (1:10) showed additional medium-strength acidic sites at ≈330 °C and strong acidic sites near 500 °C. This suggests that NA treatment significantly alters the surface acidity of TiO_2, promoting the creation of medium- and strong-strength acid sites, which are critical for enhancing catalytic activity.

Although the strength of these acidic sites appeared consistent across the NA-treated samples, the concentration of NA had a minor impact on the overall acidity. Specifically, increasing the NA concentration from 1:1 to 1:10 did not substantially affect the strength or the number of acid sites. This result is consistent with findings from Ishikawa et al. where acidic supports, irrespective of the degree of acidity, promoted enhanced catalytic performance in hydrocarbon oxidation reactions.[13] The behavior of TiO_2 under acidic conditions is governed by its PZC, which typically lies around pH 6–7.[17–19] Below this pH, the surface hydroxyl ($-OH$) groups on the TiO_2 become protonated, forming positively charged hydroxyl groups ($-OH_2^+$), leading to a net positive surface charge. This positive charge facilitates the adsorption of negatively charged Pt precursors, such as tetraamineplatinum, through electrostatic interactions. Such interactions prevent Pt precursor aggregation, thereby improving Pt dispersion on the TiO_2 surface.[16] This phenomenon is particularly critical when applying NA treatments, as it enhances the overall Pt dispersion, leading to smaller and more uniform Pt particle formation.

A surface infrared (IR) analysis was performed to further investigate the surface species following NA treatment and subsequent Pt introduction, as compared in **Figure 1**. Prior to measurement, all samples were subjected only to stirring and drying, without calcination. Catalyst backgrounds were established using KBr, and surface IR spectra were recorded after a 1 h pretreatment with nitrogen at 120 °C. The untreated TiO_2 exhibited no detectable nitrate species, indicating that nitrates were not directly immobilized on the surface, although they may have contributed to the formation of acidic sites. However, after impregnating Pt on TiO_2, distinct peaks corresponding to bidentate and bridge nitrate species emerged at 1584 and 1611 cm^{-1}, respectively.[20–23] This observation suggests that tetraamineplatinum interacts with the TiO_2 surface, where nitrate species

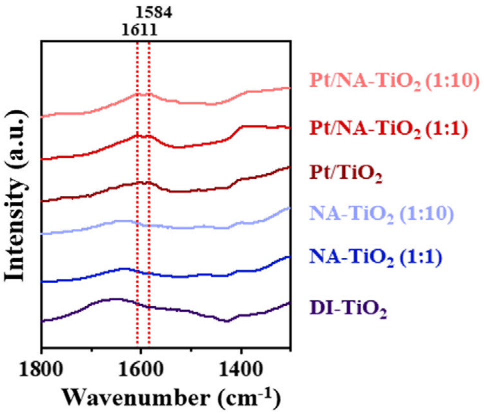

Figure 1. Diffuse reflectance infrared Fourier transform spectroscopy (DRIFT) spectra of noncalcined catalyst samples.

indirectly distributed via electrostatic interactions with the Pt precursor. Additionally, the bidentate and bridge nitrate peaks were more pronounced in the Pt/NA-TiO_2 (1:1) and Pt/NA-TiO_2 (1:10) samples compared to untreated Pt/TiO_2, indicating that the acidic sites on TiO_2 promoted more uniform Pt dispersion. The presence of acidic sites facilitates the effective adsorption of tetraammineplatinum, which leads to enhanced Pt dispersion. The enhanced acidic sites generated by NA treatment provide a more stable platform for Pt adsorption, resulting in more intense nitrate peaks. Interestingly, a slight variation in the intensity of these nitrate peaks was noted, in contrast to the NH_3-TPD data, which showed relatively constant acidity across the samples.

To further explore these surface interactions, thermogravimetric analysis (TGA) was conducted to examine the desorption behavior of surface species across different temperatures. Each sample was analyzed immediately after drying without calcination. As shown in Figure S2 in the Supporting Information, weight loss was monitored from 50 to 550 °C. The initial weight loss observed between 50 and 200 °C could be primarily attributed to the desorption of physisorbed water and loosely bound surface hydroxyl (—OH) groups.[24] In the 200–300 °C range, a weight loss of 2–3% was recorded, corresponding to the desorption of more weakly bound species from the TiO_2 surface.[25] This includes the removal of surface hydroxyl groups, corroborated by DRIFTS analysis. Additionally, during this temperature interval, the desorption of amine groups from the platinum precursor was detected. The Pt/NA-TiO_2 (1:10) sample exhibited further weight loss above 400 °C, likely due to the desorption and subsequent decomposition of surface nitrate species.[26–28]

Based on these TGA results, a surface IR study was further performed to simulate the behavior of surface species during the calcination process (**Figure 2**). Precalcined samples were analyzed with background spectra collected using KBr. Spectra were recorded from 50 to 550 °C, with a heating rate of 2 °C min^{-1} under a 20% O_2/N_2 atmosphere. The left-side graphs display spectra on a consistent intensity scale, as do the right-side graphs, enabling direct comparison. In the —OH stretching region (3750–3400 cm^{-1}), a broad peak was observed, attributed to hydroxyl groups attached to the TiO_2 surface.[29,30] The IR peak at 3400–2800 cm^{-1} reveals water complexes tightly bound to the TiO_2 surface.[31] Desorption of these water molecules and surface hydroxyl groups was detected between 250 and 300 °C. The IR peak at 1800–1400 cm^{-1} range indicates the distribution of nitrate species. As seen in Figure 1, bidentate nitrate (1584 cm^{-1}) and bridge nitrate (1611 cm^{-1}) peaks were present across all samples. These peaks stabilized around 250 °C, likely reflecting the desorption of amine groups from the platinum precursor and hydroxyl groups from TiO_2, further supporting the interaction between Pt and NO_3^-. Above 400 °C, nitrate species gradually desorbed, weakening the nitrate peaks and exposing Pt active sites on the TiO_2 surface. A notable difference in nitrate intensity was observed, particularly between Pt/NA-TiO_2 (1:1) and Pt/NA-TiO_2 (1:10). The latter displayed a lower nitrate intensity despite containing more nitrate, likely due to competitive nitrate adsorption when excessive nitrate is present in solution, reducing Pt dispersion.

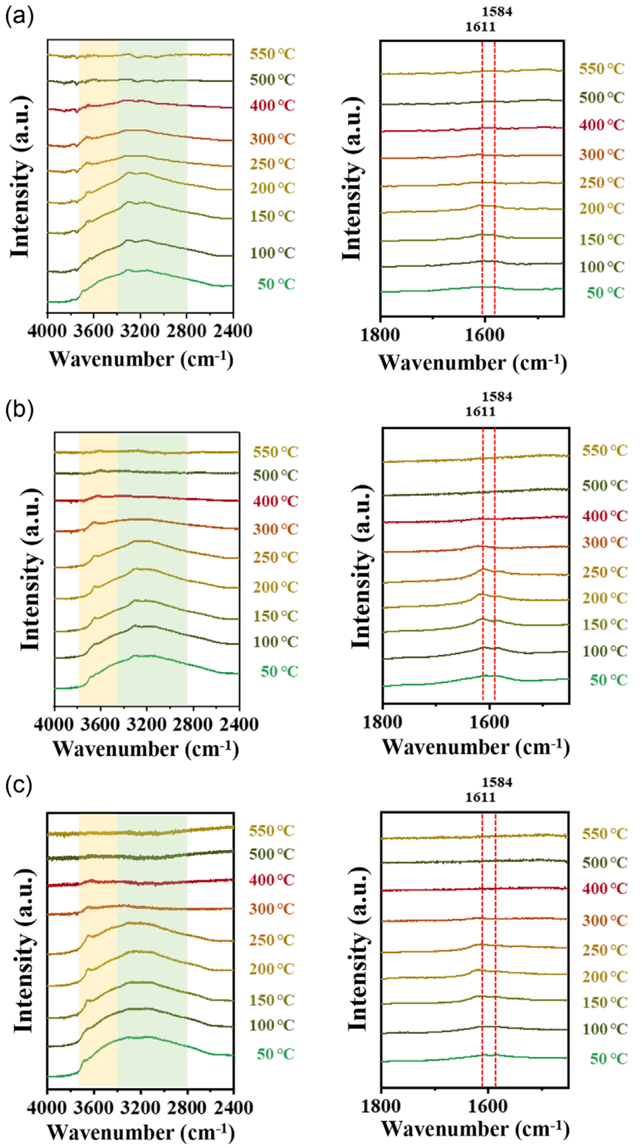

Figure 2. DRIFT spectra of a) TiO_2, b) Pt/NA-TiO_2 (1:1), and c) Pt/NA-TiO_2 (1:10) samples.

To confirm the presence of nitrate in the synthesis solution, each catalyst solution was filtered and the residual nitrate was analyzed by comparing IR spectra as shown in Figure S3, Supporting Information. HNO_3 was vaporized exclusively in the Pt/NA-TiO_2 (1:10) sample. In contrast, when lower NA concentrations were used, nitrate was predominantly adsorbed onto the catalyst surface, ensuring stable Pt precursor binding to TiO_2. Excess nitrate, however, remained in solution at higher NA concentrations. Given that nitrate is negatively charged, it can engage in electrostatic interactions with the positively charged TiO_2 surface. These interactions could lead to competitive adsorption between nitrate and the Pt precursor, reducing Pt adsorption efficiency on the TiO_2 surface. This reduction in Pt adsorption may subsequently lead to diminished Pt dispersion and particle aggregation, adversely affecting catalytic performance.

2.2. Pt Phase and Morphology

Despite the formation of similar levels of acidic sites under varying NA concentrations, a higher concentration of nitrate species was observed in the Pt/NA-TiO_2 (1:1) sample. This phenomenon is closely tied to the particle size and dispersion of Pt. Previous studies have consistently demonstrated that Pt dispersion plays a crucial role in determining catalytic performance, particularly in methane oxidation. Stakheev et al. reported that Pt/TiO_2 catalysts supported on more acidic materials exhibited superior performance in CH_4 oxidation, where catalytic activity was significantly enhanced when the Pt particle size was below 4 nm.[14] Similarly, Hansen et al. studied Pt particle sizes ranging from 1.3 to 18.7 nm in oxidation reactions, confirming that smaller particles, especially those between 2 and 4 nm, provide optimal catalytic activity.[32] These findings suggest a strong correlation between NA treatment, Pt particle size and dispersion, and overall catalyst performance in methane oxidation. To support this further, the high-resolution transmission electron microscopy was employed to compare the particle size and distribution of Pt in both Pt/TiO_2 and Pt/NA-TiO_2 samples (**Figure 3**)

For the untreated Pt/TiO_2 samples, relatively large Pt particles were observed, with an average size of 24.6 ± 15.9 nm. This is attributed to the limited number of adsorption sites on the TiO_2 surface, which impeded the uniform adsorption of the Pt precursor. Without sufficient acidic sites, the Pt precursor tended to aggregate, leading to the formation of larger particles. In contrast, the Pt/NA-TiO_2 (1:0.5) and Pt/NA-TiO_2 (1:1) samples exhibited significantly smaller particles, with sizes of 7.4 ± 4.6 and 6.3 ± 4.7 nm, respectively. As discussed, the NA treatment generates acidic sites on the TiO_2 surface, facilitating the uniform adsorption of Pt precursors and preventing agglomeration. However, in the Pt/NA-TiO_2 (1:10) sample, the particle size increased to 12.3 ± 7.5 nm, larger than those observed in the samples treated with lower concentrations of NA. This increase suggests that higher nitrate concentrations can have a detrimental effect on Pt precursor adsorption, promoting aggregation due to competitive adsorption of nitrate ions. These findings align with NH_3-TPD measurements, which indicated that excessive nitrate in solution could inhibit Pt dispersion, ultimately compromising catalytic performance.

The XRD patterns for Pt/TiO_2, Pt/NA-TiO_2 (1:1 and 1:10), DI-TiO_2, and NA-TiO_2 (1:1) are presented in Figure S4 in the Supporting Information. The strongest diffraction peak at 22.3° corresponds to the (101) plane of anatase TiO_2. Both crystal structures are observed as the support material consists of a mixture of anatase and rutile phases (TiO_2 P25). The influence of NA treatment on the TiO_2 support appears minimal. For Pt, diffraction peaks at $2\theta = 39.6°$, 47.4°, and 67.1° are assigned to the (111), (200), and (220) reflections, respectively, which match the face-centered cubic phase of Pt (JCPDS 04-0802). Notably, Pt/TiO_2 and Pt/NA-TiO_2 (1:10) exhibit relatively pronounced Pt crystalline phases compared to the TiO_2 phase, whereas Pt/NA-TiO_2 (1:1) shows less distinct Pt peaks and reduced intensity. These observations align with the transmission electron microscopy (TEM) results, indicating smaller particle sizes and improved dispersion in the Pt/NA-TiO_2 (1:1) sample.

The phase and oxidation states of Pt particles were identified by X-Ray photoelectron spectroscopy (XPS) over a series of Pt/TiO_2 and Pt/NA-TiO_2 catalysts, as presented in **Figure 4**. The Pt^0 state was detected at a binding energy near 70.6 eV, Pt^{2+} at 72.8 eV, and Pt^{4+} near 74.6 eV, with a spin-orbit splitting of 3.35 eV. The binding energies and the relative ratio of Pt oxidation states for each sample are summarized in **Table 1**. In both precalcined Pt/TiO_2 and Pt/NA-TiO_2 samples, the Pt^{2+} is the main state of Pt sites. This is attributed to the tetraamineplatinum precursor used for catalyst preparation. After calcination, however, differences in Pt oxidation states were observed, particularly in Pt/NA-TiO_2 (1:0.5) and Pt/NA-TiO_2 (1:1) samples treated with moderate amounts of NA. These samples showed

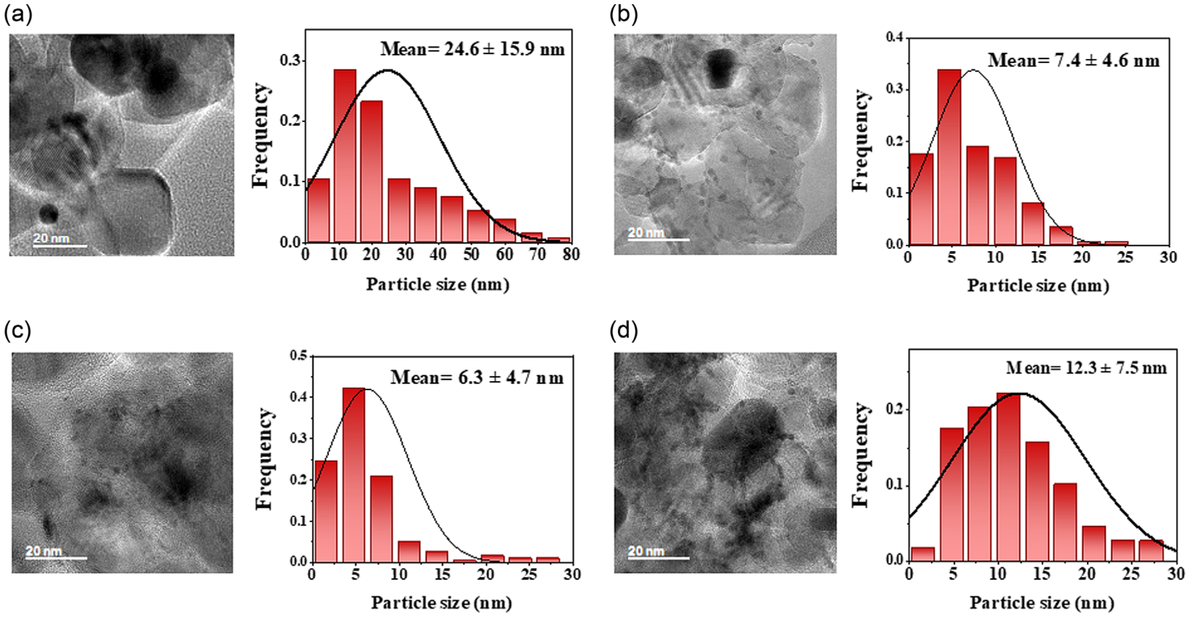

Figure 3. TEM images and corresponding particle size distribution of a) Pt/TiO_2, b) Pt/NA-TiO_2 (1:0.5), c) Pt/NA-TiO_2 (1:1), and d) Pt/NA-TiO_2 (1:10).

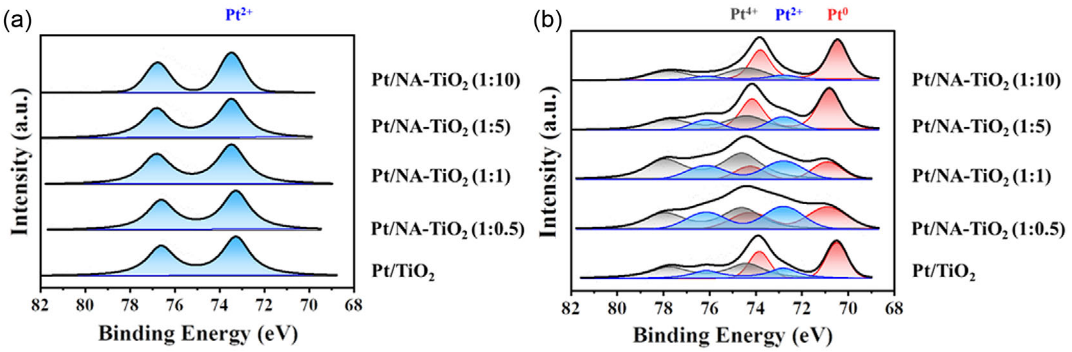

Figure 4. Pt 4f XPS spectra of Pt/TiO$_2$ and Pt/NA-TiO$_2$ a) before calcination b) after calcination.

Table 1. Quantitative analysis of Pt 4f XPS.

Catalysts	Binding energy [eV]			Surface atomic concentration [%]		
	Pt^0	Pt^{2+}	Pt^{4+}	Pt^0	Pt^{2+}	Pt^{4+}
Pt/TiO$_2$	70.5	72.8	74.4	39.6	22.1	38.3
Pt/NA-TiO$_2$ (1:0.5)	70.9	72.8	74.6	31	31.9	37.1
Pt/NA-TiO$_2$ (1:1)	70.9	72.8	74.6	27.4	34.8	37.8
Pt/NA-TiO$_2$ (1:5)	70.8	72.8	74.4	51.9	17.8	30.3
Pt/NA-TiO$_2$ (1:10)	70.5	72.8	74.4	57.8	13.9	28.3

a decrease in the Pt^0 ratio and an increase in the Pt^{2+} ratio compared to untreated Pt/TiO$_2$, indicating that the acidic sites formed through NA treatment promoted stronger interactions between Pt and the TiO$_2$ surface, leading to partial oxidation of Pt. This observation is supported by surface IR results, which confirm the formation of stable interactions between Pt and the acidic sites on TiO$_2$.

Pt/NA-TiO$_2$ (1:5) and Pt/NA-TiO$_2$ (1:10) samples treated with higher concentrations of NA, exhibited a sharp increase in the Pt^0 state and a decrease in the Pt^{2+} state. This shift is likely due to competitive adsorption of excess nitrate ions on the TiO$_2$ surface, which inhibited the stable binding of Pt precursors, thereby preventing full oxidation and leading to a higher prevalence of metallic Pt^0. These changes in the Pt oxidation state reflect the complex interplay between NA concentration and Pt precursor adsorption during catalyst preparation. While Pt^0 is often considered the primary active site for methane oxidation, its oxidized forms, such as Pt^{2+}, can be reduced back to the metallic state at elevated temperatures (above 400 °C) during catalytic reactions. Since methane oxidation typically occurs at temperatures exceeding 500 °C, the exact oxidation state of Pt may play a less direct role in catalytic performance at these high temperatures. Instead, Pt particle size and dispersion could impact overall catalyst efficiency. Therefore, optimizing the conditions to achieve favorable Pt dispersion and particle size is critical for improving catalytic performance for high-temperature methane oxidations.

2.3. Catalytic CH$_4$ Oxidation Performance

We confirmed the redox properties of the catalysts through hydrogen temperature-programmed reduction (H$_2$-TPR) analysis as presented in **Figure 5**, where two main reduction steps were observed. In the low-temperature range (300–400 °C), a peak corresponding to the reduction of Pt^{2+} to Pt^0 was detected. In the high-temperature range (400–500 °C), the reduction of Pt^{4+} to lower oxidation states (Pt^{2+} and Pt^0) occurred, attributed to the interaction between Pt and the TiO$_2$ support. Notably, the Pt/NA-TiO$_2$ (1:1) sample exhibited well-defined reduction peaks for both Pt^{2+} and Pt^0, indicating high Pt dispersion. The reduction of Pt^{2+} to Pt^0 in this sample is identified as crucial factor for optimizing the catalyst's redox performance. In contrast, the Pt/NA-TiO$_2$ (1:10) sample showed a weakened Pt^{2+} reduction peak and reduced H$_2$ consumption, suggesting that excessive NA treatment resulted in lower Pt dispersion and decreased catalytic performance.

The methane oxidation performance was evaluated over a series of Pt/TiO$_2$ catalysts synthesized by varying the NA treatment. **Figure 6** compares CH$_4$ conversions from 350 to 550 °C under a 5% water vapor-containing condition. It was confirmed that the selectivity of methane oxidation to CO$_2$ was 100% overall catalyst samples. The CH$_4$ conversion of the Pt/TiO$_2$ catalyst without NA treatment was less than 10% at 500 °C, demonstrating that typical impregnation of Pt on TiO$_2$ is not effective in the methane oxidation. However, the Pt/NA-TiO$_2$ samples treated with NA in the range of 1:0.1 to 1:1 of Pt:NA ratios showed significant methane conversions, ≈70% at 550 °C. As discussed in Section 3.2, moderate NA treatment enhances the protonation of

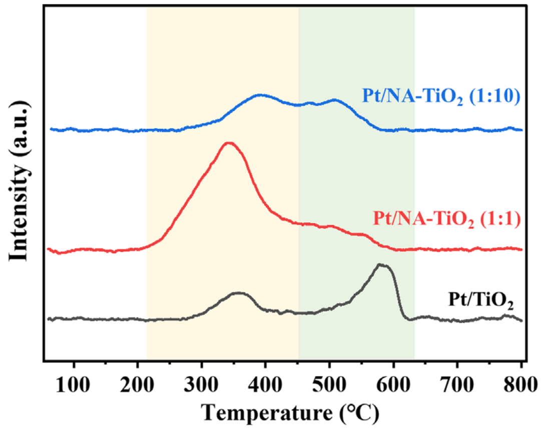

Figure 5. H$_2$-TPR of Pt/TiO$_2$, Pt/NA-TiO$_2$ (1:1), and Pt/NA-TiO$_2$ (1:10).

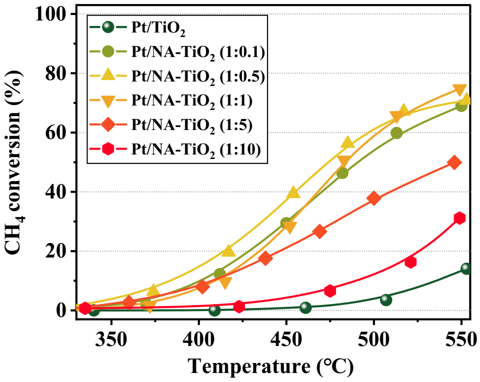

Figure 6. Catalytic CH_4 oxidation performance over Pt/TiO_2 and Pt/NA-TiO_2 (1:0.1–10). The gas mixture of 0.2% CH_4, 5% O_2, 5% H_2O, and N_2 as the balance gas, at a gas hourly space velocity (G.H.S.V.) of 100 000 h^{-1}.

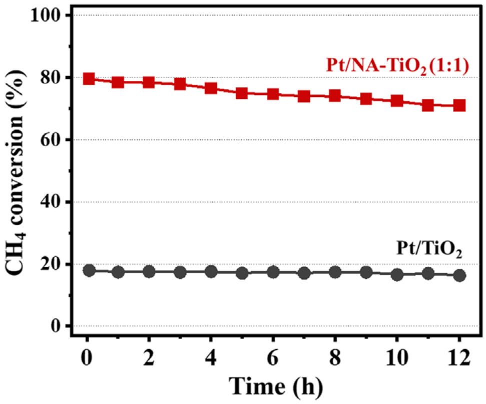

Figure 7. Long-term catalytic activity over Pt/TiO_2 and Pt/NA-TiO_2 (1:1) for 12 h at 550 °C. The gas mixture of 0.2% CH_4, 5% O_2, 5% H_2O, and N_2 as the balance gas, at a gas hourly space velocity (G.H.S.V.) of 100 000 h^{-1}.

the TiO_2 surface, creating effective adsorption sites for the Pt precursor, which improves Pt dispersion and results in smaller particle sizes. Conversely, the Pt/NA-TiO_2 (1:5) and (1:10) samples with excessive NA treatments exhibited decreased catalytic performances. This also aligns with previous observations regarding surface adsorbates, morphology, and surface changes induced by NA, indicating that excessive treatment degrades Pt dispersion.

The long-term stability test in **Figure 7** demonstrated that the Pt/NA-TiO_2 (1:1) catalyst exhibited a stable catalytic activity for methane oxidation, maintaining 70–80% of methane conversion for 12 h. In contrast, Pt/TiO_2 exhibited significantly lower activity, only around 20% of methane conversion. The optimized NA treatment improves catalytic performance by enhancing Pt dispersion and reducing particle size on the TiO_2 surface and it also confirmed superior long-term stability.

3. Conclusion

This study confirmed the critical role of NA treatment in tailoring the surface properties and catalytic behavior of Pt/TiO_2 catalysts for methane oxidation. Through a systematic exploration of various NA concentrations, we demonstrated that controlled acid treatment (1:0.1 to 1:1 of Pt:NA) significantly enhances Pt particle dispersion, increases surface acidity, and ultimately improves methane oxidation performance. However, excessive NA concentrations (above 1:5 of Pt:NA) adversely affect these properties by promoting Pt aggregation and reducing dispersion, which diminishes catalytic efficiency.

This relationship between Pt particle size, dispersion, and catalytic activity underscores the necessity of carefully balancing acid treatment to achieve optimal performance. Furthermore, the study provides insights into the interaction between Pt and nitrate species, where NA treatment affects the adsorption mechanisms and particle stability on TiO_2. Such interactions are pivotal for improving not only methane oxidation but also other oxidation reactions involving Pt-based catalysts.

The comprehensive characterization techniques, including XPS, TEM, and DRIFTS, revealed the structural and electronic changes induced by NA treatment, offering pathways for further catalyst optimization. These findings serve as a simple methodology for designing Pt supported on TiO_2 catalysts in broader environmental and industrial applications, particularly in addressing the aftertreatment of methane emissions.

4. Experimental Section

Catalyst Preparation: Titanium dioxide (TiO_2), a mixture of rutile and anatase phases (Sigma-Aldrich), was used as the support material for catalyst synthesis. A 70% NA solution (HNO_3; Sigma-Aldrich) was employed for the NA treatment to modify the surface properties of TiO_2. The TiO_2 support was suspended in DI water and treated with the NA solution under continuous stirring at room temperature for 30 min, ensuring that no evaporation occurred during the process. The NA was introduced at specific molar ratios to platinum (1:0, 1:0.5, 1:1, 1:5, and 1:10) to adjust the surface acidity and create acidic sites on the TiO_2 surface. Following this, the platinum precursor, tetraamineplatinum(II) nitrate ($[Pt(NH_3)_4](NO_3)_2$; Sigma-Aldrich), was impregnated, equivalent with 3 wt% of Pt loading. The mixture was stirred at 80 °C for 12 h to evaporate the solvent and promote uniform dispersion of Pt onto the acid-treated TiO_2. The resulting powder was then dried at 120 °C for 4 h and calcined at 550 °C for 6 h in air using a muffle furnace, ensuring complete removal of moisture and thorough formation of the Pt/TiO_2 and Pt/NA-TiO_2 catalysts.

Catalytic Characterization: TGA was performed using a TGA-50 instrument (SHIMADZU) to analyze the thermal behavior of the catalysts during calcination. ≈10 mg of each sample was heated from 30 to 800 °C at a rate of 20 °C min^{-1} under a nitrogen atmosphere. Surface infrared analysis was conducted using *in situ* DRIFTS to identify surface intermediates. For surface IR analysis, a NICOLET iS50 FT-IR (Thermo Fisher Scientific) equipped with an MCT detector and a DRIFTS reaction cell (DiffusIR, PIKE Technologies, with a ZnSe window and a 10 s scanning time) was used. Surface IR studies were performed at room temperature to examine the catalyst surface. Additionally, in situ DRIFTS was conducted under a 20% O_2/N_2 balance, with measurements taken from 50 to 550 °C, to simulate the calcination process and identify surface intermediates.

The morphology and structure of the catalysts were observed using HR-TEM (FEI) at 300 kV. For elemental mapping, high-angle annular dark-field scanning transmission electron microscopy was employed in conjunction with a Super-X energy-dispersive X-Ray spectroscopy system.

XPS analysis (NEXSA, Thermo Fisher Scientific) was conducted to examine the valence states of Pt 4f on the catalyst surface. The binding energy was calibrated using the 284.8 eV peak of surface adventitious C 1s. The Shirley algorithm was utilized to determine the spectrum boundary condition.

NH_3-TPD and H_2-TPR were both conducted using a Microtrac Belcat II instrument. For NH_3-TPD, the catalysts were pretreated in a 10% O_2/He environment at 500 °C for 1 h, followed by cooling to room temperature in a He atmosphere. The sample was then heated to 700 °C, and desorbed ammonia was monitored using a thermal conductivity detector (TCD). For H_2-TPR, the sample was pretreated in Ar at 500 °C for 1 h, followed by 10% O_2/Ar pretreatment. After cooling to 50 °C, the sample was heated to 800 °C, and hydrogen consumption was monitored using a TCD.

Catalytic Activity Test: Catalytic performances were tested in a tubular quartz reactor heated by a temperature-programmed electric tubular furnace to control the reactor temperature. The sieved catalyst was placed in the reactor, and held in place by quartz wool. Prior to the activity tests, the catalysts were pretreated at 500 °C for 1 h in a gas mixture containing 5% O_2 and 5% H_2O, with N_2 as the balance gas, then cooled to 300 °C under N_2-only conditions. Steady-state CH_4 oxidation performance was measured from 300 to 550 °C in 40 °C intervals, with a 30-minute hold at each step and a ramp rate of $10\,°C\,min^{-1}$ under simulated exhaust conditions. The gas mixture contained 0.2% CH_4, 5% O_2, 5% H_2O, and N_2 as the balance gas, with a gas hourly space velocity (G.H.S.V.) of $100\,000\,h^{-1}$. DI water was injected into the reactor using a programmable syringe pump (NE-1000, New Era Pump Systems) and evaporated at 160 °C through a preheater system installed at the reactor inlet. All gas lines connected to the reactor were maintained at 160 °C to prevent water condensation. The concentrations of CH_4 and CO_2 were measured using a Fourier transform infrared spectroscopy gas analyzer (Perkin-Elmer Spectrum 2) equipped with a 5-m Long-Path Gas Cell (PIKE Technologies) at a resolution of $2\,cm^{-1}$.

Supporting Information

Supporting Information is available from the Wiley Online Library or from the author.

Acknowledgements

This work was supported by the National Research Foundation of Korea (NRF) grant funded by the Korea Government (MSIT) (no. 2021R1A5A1028138, 2021R1C1C1005404, and RS-2023-00282392).

Conflict of Interest

The authors declare no conflict of interest.

Author Contributions

Jiseok Park: data curation (lead); formal analysis (lead); investigation (lead); writing—original draft (lead). **Wo Bin Bae**: formal analysis (equal); investigation (equal); methodology (equal). **Sang Woo Byun**: data curation (equal); formal analysis (equal); methodology (equal). **Hyeonwoo Shin**: data curation (equal); formal analysis (equal). **Haehyun Min**: formal analysis (equal); investigation (equal); methodology (equal). **Young Jin Kim**: formal analysis (equal); investigation (equal); methodology (equal). **Sung Bong Kang**: conceptualization (lead); funding acquisition (lead); supervision (lead); writing—review and editing (lead).

Data Availability Statement

The data that support the findings of this study are available from the corresponding author upon reasonable request.

Keywords

CH_4 oxidations, dispersion and phase, nitric acid treatments, Pt/TiO_2, surface acidity

Received: October 23, 2024
Revised: November 20, 2024
Published online:

---

[1] P. Briot, M. Primet, *Appl. Catal.* **1991**, *68*, 301.
[2] P. Gélin, L. Urfels, M. Primet, E. Tena, *Catal. Today* **2003**, *83*, 45.
[3] O. Mihai, G. Smedler, U. Nylén, M. Olofsson, L. Olsson, *Catal. Sci. Technol.* **2017**, *7*, 3084.
[4] D. Ciuparu, L. Pfefferle, *Appl. Catal. A: Gen.* **2001**, *209*, 415.
[5] S. Ballauri, E. Sartoretti, M. Hu, C. D'Agostino, Z. Ge, L. Wu, C. Novara, F. Giorgis, M. Piumetti, D. Fino, N. Russo, S. Bensaid, *Appl. Catal. B: Environ.* **2023**, *320*, 121898.
[6] Q. Li, Y. Wang, W. Si, Y. Peng, J. Li, *ACS Appl. Mater. Interfaces* **2023**, *15*, 7959.
[7] N. M. Kinnunen, J. T. Hirvi, M. Suvanto, T. A. Pakkanen, *J. Mol. Catal. A: Chem.* **2012**, *356*, 20.
[8] R. Hicks, *J. Catal.* **1990**, *122*, 280.
[9] R. Burch, P. K. Loader, F. J. Urbano, *Catal. Today* **1996**, *27*, 243.
[10] E. D. Goodman, S. Dai, A.-C. Yang, C. J. Wrasman, A. Gallo, S. R. Bare, A. S. Hoffman, T. F. Jaramillo, G. W. Graham, X. Pan, M. Cargnello, *ACS Catal.* **2017**, *7*, 4372.
[11] K. A. Miki Niwa, Y. Murakami, *Appl. Catal.* **1983**, *7*, 317.
[12] N. G. C. Bozo, *Catal. Today* **2000**, *59*, 33.
[13] S. I. K. Akiko Ishikawa, A. Satsuma, T. Hattori, Y. Murakami, *Appl. Catal. A: Gen.* **1994**, *110*, 61.
[14] A. Y. Stakheev, I. E. Beck, G. O. Bragina, V. I. Zaikovsky, A. B. Ayupov, N. S. Telegina, V. I. Bukhtiyarov, *Russ. Chem. Bull.* **2010**, *59*, 1713.
[15] J. P. Holmberg, E. Ahlberg, J. Bergenholtz, M. Hassellov, Z. Abbas, *J. Colloid Interface Sci.* **2013**, *407*, 168.
[16] W. B. Bae, J. Park, Y. J. Go, S. W. Byun, H. Shin, Y. J. Kim, J. H. Jang, S. B. Kang, *Sep. Purif. Technol.* **2025**, *357*, 130033.
[17] J.-C. Chou, L. P. Liao, *Thin Solid Films* **2005**, *476*, 157.
[18] H. He, Y. Cheng, C. Yang, G. Zeng, C. Zhu, Z. Yan, *J. Environ. Sci.* **2017**, *54*, 135.
[19] C. Xiang, F. Yang, M. Li, M. Jaridi, N. Wu, *J. Nanopart. Res.* **2012**, *15*, 1293.
[20] X. Zhang, H. He, H. Gao, Y. Yu, *Spectrochim. Acta A Mol. Biomol. Spectrosc.* **2008**, *71*, 1446.
[21] S. Tamm, N. Vallim, M. Skoglundh, L. Olsson, *J. Catal.* **2013**, *307*, 153.
[22] P. Sazama, L. Capek, H. Drobna, Z. Sobalik, J. Dedecek, K. Arve, B. Wichterlova, *J. Catal.* **2005**, *232*, 302.
[23] M. Y. Mihaylov, V. R. Zdravkova, E. Z. Ivanova, H. A. Aleksandrov, P. S. Petkov, G. N. Vayssilov, K. I. Hadjiivanov, *J. Catal.* **2021**, *394*, 245.
[24] Y. Tian, Y. Li, X. Xu, Z. Jin, *Carbohydr. Polym.* **2011**, *84*, 1165.
[25] A. Bondarev, D. R. Popovici, C. Calin, S. Mihai, E. E. Sirbu, R. Doukeh, *Materials* **2023**, *16*, 4285.
[26] J. S. X. Chen, J. Li, W. F. Schneider, C. T. Goralski, P. J. Schmitz, *Appl. Catal. B: Environ.* **2005**, *61*, 164.
[27] M. D. T. Venkov, K. Hadjiivanov, *J. Mol. Catal. A: Chem.* **2006**, *243*, 8.
[28] K. S. C. Sedlmair, A. Jentys, J. A. Lercher, *J. Catal.* **2003**, *214*, 308.
[29] T. Bezrodna, G. Puchkovska, V. Shymanovska, J. Baran, H. Ratajczak, *J. Mol. Struct.* **2004**, *700*, 175.
[30] H. Lin, J. Long, Q. Gu, W. Zhang, R. Ruan, Z. Li, X. Wang, *Phys. Chem. Chem. Phys.* **2012**, *14*, 9468.
[31] D. A. Panayotov, J. T. Yates, *Chem. Phys. Lett.* **2005**, *410*, 11.
[32] T. K. Hansen, B. B. Hansen, M. Høj, T. V. W. Janssens, A. D. Jensen, *Top. Catal.* **2017**, *60*, 1333.